Competitive reaction pathways of C_2Cl_3 + NO via four-membered ring and bicyclic ring intermediates†

Kunhui Liu,[a] Di Song,[a] Shaolei Zhao,[a] Sufan Wang,[b] Chunfan Yang[a] and Hongmei Su*[a]

Received 15th July 2010, Accepted 20th September 2010
DOI: 10.1039/c0cp01192d

The products and mechanisms of the atmospherically and environmentally important reaction, C_2Cl_3 + NO, are investigated comprehensively by step-scan time-resolved Fourier transform infrared emission spectroscopy and the CCSD(T)/6-311+G(d)//B3LYP/6-311G(d) level of electronic structure calculations. Vibrationally excited products of Cl_2CO, ClNCO, CCl_3NCO and NCO have been observed in the IR emission spectra. Cyclic intermediates are found to play important roles leading to the rich variety of the chemical transformations of the reaction. Mainly two competitive reaction pathways are revealed: the four-membered ring intermediate pathway leading to the products Cl_2CO + ClCN which is essentially barrierless and the bicyclic ring intermediate pathway leading to the product channels of ClNCO + CCl_2, CCl_3NCO and CCl_3 + NCO which is rate-limited by a barrier of 42.9 kJ mol^{-1} higher than the reactants. By photolyzing the precursor at 248 and 193 nm, respectively, C_2Cl_3 radicals with different internal energy are produced to observe the product branching ratios as a function of reactant energy. The Cl_2CO channel *via* the four-membered ring intermediate pathway is shown to be overwhelmingly dominant at low energy (temperature) but become less important at high energy while the ClNCO and CCl_3NCO channels *via* the bicyclic ring intermediate pathway are greatly enhanced and compete effectively. The experimental observation of the products and their branching ratios varying with reactant energy is well consistent with the calculated potential energy profiles.

Introduction

The chlorinated radical is known to be among intermediates of the combustion of chlorinated hydrocarbons (CHCs) which are commonly found in the environment because they are widely used as an effective, yet relatively non-flammable solvents, unlike kerosene or gasoline.[1,2] The trichlorovinyl radical, C_2Cl_3, has been demonstrated to be involved in the most important and sensitive reactions in a number of systems of burning and pyrolysis of chlorine-rich unsaturated CHCs, especially during the incineration of municipal solid waste (MSW) such as poly(vinyl chloride).[3,4] Meanwhile, nitrogen oxides (NO_x) are also the generally acknowledged pollutants emitting from the burning process of CHCs, which are known to react rapidly with free radicals and such reactions are thought to suppress soot formation.[5] Despite the prominence of the C_2Cl_3 radical in combustion chemistry and environmental chemistry, investigations of its reaction mechanisms and kinetics have been relatively scarce. The reaction kinetics of C_2Cl_3 with molecular oxygen was first measured by Russell *et al.* in 1989 using a tubular flow tube reactor coupled with a photoionization mass spectrometer (PIMS) in the temperature range 298–648 K.[6] Another reported kinetics measurement was the reaction of C_2Cl_3 with Cl_2 by Knyazev *et al.* and the reaction rate constants were obtained to be $k = 3.79 \times 10^{-15} T^{0.87} \exp(-55\ \mathrm{K}/T)$ cm^3 molecule^{-1} s^{-1}.[7] As a serial work prior to this study, we have studied the reaction products and mechanisms of C_2Cl_3 radical with O_2 and NO_2 theoretically and experimentally.[8–11]

Although there has been a lack of investigation concerning the title reaction C_2Cl_3 + NO, sufficient information can be retrieved from the literature for its counterpart reaction C_2H_3 + NO which may provide valuable hints for the current work.[12–18] In early experiments performed in the context of the mercury-photosensitized decomposition of acetylene/NO mixtures[13] and H or Cl initiated reactions of acetylene with NO,[12] Sherwood and Gunning observed that HCN and H_2CO are the dominant products of the C_2H_3 + NO reaction at room temperature and suggested that the reaction proceeds through an OCCN four-membered ring intermediate (1,2-oxazete) followed by N–O and C–C bond breaking. Later, this mechanism was confirmed in the *ab initio* calculations by Sumathi *et al.*[16] using the methods of MP2 and CCSD(T) with the 6-311++G(d,p) basis set. However, this calculation also predicted that the C_2H_3 + NO reaction can not proceed beyond the four-membered ring oxazete intermediate at room temperature due to a high barrier for dissociation of the oxazete intermediate and hence the products HCN + H_2CO

[a] *State Key Laboratory of Molecular Reaction Dynamics, Beijing National Laboratory for Molecular Sciences (BNLMS), Institute of Chemistry, Chinese Academy of Sciences, Beijing 100190, China. E-mail: hongmei@iccas.ac.cn*
[b] *College of Chemistry and Materials Science, Anhui Normal University, Wuhu 241000, China*

† This article was submitted as part of a special collection of papers from the Institute of Chemistry, Chinese Academy of Sciences (ICCAS).

can only become significant at high temperature. This is obviously in contradiction with the earlier experimental observation of Sherwood and Gunning.[12,13]

Such discrepancies have been well resolved by two recent theoretical and experimental works. Striebel *et al.*[17] performed *ab initio* calculations at the QCISD(T) and the multi-reference configuration interaction (MRCI) level, providing a higher level quantum chemical analysis of the key stationary points on the C_2H_3 + NO potential energy surface. The net result was a confident prediction that the pathway to forming HCN + H_2CO has a maximum barrier that lies well below the reactants (62.8 kJ mol^{-1} below), substantially lower than in the previous results of Sumathi *et al.*[16] Their RRKM master equation calculations based on these lower barrier heights satisfactorily reproduced the measured temperature and pressure dependence of the rate coefficient. The calculated rate coefficient drops too slowly with decreasing pressure, indicating that the reaction does not terminate at the 1,2-oxazete four-membered ring intermediate, but proceeds by the 1,2-oxazete dissociation to form final products HCN + H_2CO. In addition, another low energy pathway producing H_2CNH + CO through a bicyclic intermediate was also predicted in their calculations. Subsequent to this work, Osborn *et al.*[18] identified unambiguously the products H_2CO and HCN by time-resolved Fourier transform emission spectroscopy and determined that HCN + H_2CO *via* the dissociation of four-membered ring intermediate is the only significant product channel for the C_2H_3 + NO reaction near room temperature. Other possible reaction pathways forming H_2CNH + CO *via* the bicyclic intermediate was indicated to be much less competitive based on the absence of the bimolecular reaction products CO in the IR spectra and a predicted upper bound of 0.19% branching ratio of this channel from RRKM calculations.

It was shown in previous investigations that the only observed significant reaction pathway for the C_2H_3 + NO reaction involves the production of HCN + H_2CO *via* the four-membered ring intermediate 1,2-oxazete,[18] although there also exist other low energy pathways *via* a variety of reactive intermediates (nearly 26 bound, topologically different C_2H_3NO isomers were identified to be relevant to the C_2H_3 + NO reaction channel).[16] For the C_2Cl_3 + NO reaction subject to study in this work, the question arises whether the reaction products and mechanisms are analogous to that of C_2H_3 + NO or not. In particular, are there any reaction pathways *via* intermediates, such as the bicyclic intermediate, in competition with the seemingly dominant four-membered ring intermediate pathway for the C_2Cl_3 + NO reaction? In this work, we are motivated to investigate the competitive pathways of the C_2Cl_3 + NO reaction resulting from the rich variety of the cyclic reactive intermediates possibly involved in the reaction due to the rich valence variation of N atom in NO and the lone pair electrons in the N and O atoms. Electronic structure calculations at the CCSD(T)/6-311+G(d)// B3LYP/6-311G(d) level are performed to analyze the key stationary points on the C_2Cl_3 + NO potential energy surface and predict the feasible reaction pathways. Experimentally, vibrationally excited products of Cl_2CO from the four-membered ring intermediate pathway and ClNCO, NCO and CCl_3NCO arising from the bicyclic ring intermediates have been detected by means of step-scan time-resolved Fourier transform infrared emission (TR-FTIR) spectroscopy. By adjusting the precursor photolysis wavelength, C_2Cl_3 radicals with different internal energy are produced to observe the product branching ratios varying with energy among competitive reaction pathways, providing further experimental evidence of the four-membered and bicyclic ring intermediates as the key reaction steps leading to these products.

Computational and experimental methods

Theoretically, the geometries of the reactants, products, various intermediates, and transition states are optimized without any symmetry constraint using the hybrid density functional theory, *i.e.*, Becke's three-parameter nonlocal exchange functional with the nonlocal correlation functional of Lee–Yang–Parr (B3LYP) with the 6-311G(d) basis sets.[19,20] For the current reaction involving seven heavy atoms, the B3LYP/6-311G(d) level of theory is a balanced method considering the computational efficiency and accuracy. Harmonic vibrational frequencies and the zero-point energies (ZPE) are calculated at the same level of theory with the optimized geometries. The intermediates are characterized by all the real frequencies while the transition states possess one and only one imaginary frequency. Connections of the transition states between two local minima have been confirmed by intrinsic reaction coordinate (IRC) calculations at the B3LYP/6-311G(d) level.[21] To obtain more accurate relative energetic information, single-point electronic energies using coupled-cluster theory, which includes all single and double excitations plus preservative corrections for triples, CCSD(T)/6-311+G(d), are calculated using the B3LYP/6-311G(d) optimized geometries. All of the theoretical calculations are performed with the Gaussian 03 program package.[22]

Experimentally, the reaction products are monitored by step-scan, time-resolved Fourier transform emission spectroscopy which has been described in detail elsewhere.[23] The instrument comprises a Nicolet Nexus 870 step-scan FTIR spectrometer, an excimer laser (Lambda Physik CompexPro 102F), a pulse generator (Stanford Research DG535) to initiate the laser pulse and achieve synchronization of the laser with data collection, two digitizers (internal 100 kHz 16-bit digitizer and external 100 MHz 14-bit GAGE CS14100 digitizer) which offer fast time resolution and a wide dynamic range as needed, and a personal computer to control the whole experiment. A liquid-nitrogen cooled InSb detector is used in this experiment. The reaction is initiated in a stainless steel flow reaction chamber in which a pair of parallel multi-layer coated mirrors reflect the UV laser beam multiple times to increase the photolysis zone. C_2Cl_3 radicals are generated by photodissociation of C_2Cl_4 at 248 nm or 193 nm. Samples of C_2Cl_4 ($\geq$ 99%) and NO ($\geq$ 99.5%) enter the flow chamber 1 cm above the photolysis beam *via* needle valves. The chamber is pumped by an 8 L s^{-1} mechanical pump and the stagnation pressure of the chamber is measured by a MKS capacitance manometer. The constant pressure of sample is maintained by adjusting the pumping speed and the needle

valves. Typically, C_2Cl_4 (10 Pa) and NO (60 Pa) are used to keep pseudo-first-order reaction conditions. Transient infrared emission is collected by a pair of gold-coated Welsh-Cell spherical mirrors and collimated by a CaF_2 lens to the step-scan TR-FTIR spectrometer. The flow rate is fast enough to replenish the sample at each laser pulse running normally at a repetition rate of 10 Hz as described in detail previously.[9]

Results and discussion

Computational results and possible reaction pathways

Theoretical calculations are first performed to predict the possible reaction products and mechanisms. By exploring the energies and geometries of the major intermediates and transition states on its lowest singlet potential energy surface, the minimum energy reaction paths for the energetically accessible product channels are obtained for the reaction of C_2Cl_3 radical with NO. Geometries of the reactants, products, various intermediates, and transition states are optimized at the B3LYP/6-311G(d) level and their single-point energies are refined at the CCSD(T)/6-311+G(d) level using the B3LYP/6-311G(d) optimized geometries. Fig. 1 and 2 present, respectively, the optimized geometries and energy diagram of the key intermediates and transition states along the potential energy surface. For conciseness, only the energetically accessible reaction routes related to the formation of the reaction products are displayed. As shown in Fig. 2, the predicted heats of reaction based on the CCSD(T)/6-311+G(d)//B3LYP/6-311G(d) level of calculation agree well with the experimental values, suggesting that the present computational method is expected to provide reliable energetic and mechanistic information for the C_2Cl_3 + NO reaction.

Initial association

As exhibited in Fig. 2, the C_2Cl_3 + NO reaction is an addition–elimination reaction starting with the barrierless addition of NO to C_2Cl_3 radicals by the N-attack mode which leads to the planar trichloro(nitroso)ethylene with two conformations, *trans*-$Cl_2C^1{=}C^2Cl$–NO (IM1) and *cis*-$Cl_2C^1{=}C^2Cl$–NO (IM2) (C^1, C^2 are labelled in order to distinguish the two different C atoms). Meanwhile, the energized *trans*-IM1 can readily undergo *trans–cis* rearrangement to *cis*-IM2 through the rotation of terminal N–O bond *via* the low barrier transition state TS1. In view of the bond lengths of IM1/IM2, the C–C bond and N–O bond are still strong double bonds. The energy of IM1 is 192.6 kJ mol^{-1} lower than that of the reactants, while IM2 is 167.4 kJ mol^{-1} lower, indicating that the initial adduct *trans*-IM1 is slightly more stabilized but the *cis*-IM2 is more reactive, from which three different ring intermediates are encountered, and then several reaction channels are open.

Pathway *via* four-membered ring intermediate IM3

From the initial adduct IM2, there is a four-membered ring closure route leading to the intermediate IM3 *via* transition state TS2. During this process, the dangling terminal O atom of IM2 approaches to the C^1 atom forming the four-membered ring IM3 with the N–O bond and C–C bond elongated to a single bond. The four-membered ring CCNO of IM3 is nearly planar but the isolated C–Cl bonds are pointed out of the plane, and thus, IM3 has no symmetry. Through transition state TS3, the C–C bond and N–O bond of the four-membered ring of IM3 are broken simultaneously forming the products Cl_2CO + ClCN. The energy of the products is 397.0 kJ mol^{-1} lower than that of the reactants indicating this reaction route is a highly exothermic process and the products, Cl_2CO and ClCN, should be vibrationally excited, which should aid experimental detection by TR-FTIR emission spectroscopy.

Pathways *via* bicyclic ring intermediate IM4

The second reaction route starts from the isomerization of the adduct IM2 to a bicyclic ring intermediate IM4 through the transition state TS4 lying 42.9 kJ mol^{-1} higher than the reactants, which is the rate-determining step for this route. With the N–O bond lengthened to 1.564 Å and the C–C bond to 1.472 Å in the bicyclic ring intermediate IM4, both the two bonds have been weakened to single bonds. Subsequently, the C–C and N–O bond break readily through the transition state TS5 with a small energy barrier, forming the isomer IM5 (*N*-chloroformylcarbonimidoyl dichloride). The highly energized IM5 can then undergo rearrangement and fragmentation further, leading to three thermodynamically feasible reaction product channels as shown in Fig. 2.

The most facile rearrangement of IM5 is the formation of a new four-membered ring intermediate IM6 *via* the transition state TS6. It should not be confused with the analogous structure of IM3. In fact, the four-membered ring sequence of IM6 is COCN which is different from the CCNO sequence of the IM3. Interestingly, IM6 can also decompose to the products of Cl_2CO + ClCN through the transition state TS7 with the fission of C^1–N and C^2–O bonds of the COCN ring, which has happened to the earlier discussed four-membered ring IM3. That is, although the sequences of the two four-membered ring intermediates are different, their further decomposition products are identical.

The second rearrangement of IM5 is the Cl atom shift from C^2 to C^1 forming trichloromethyl isocyanate CCl_3NCO (IM7) through transition state TS8. CCl_3NCO is a stable molecule existing at room temperature which is always accompanied by minor IM5 through structural isomerization. Due to its stability, IM7 can be observed as a final product or undergo further rearrangement by changing the sequence of the terminal NCO group to C(N)O to form the intermediate $CCl_3C(N)O$ (IM8) which is followed by a facile decomposition to the end products CCl_3 + NCO owing to its unstable character. In contrast, the anticipated product CCl_3 + NCO from the direct fission of C–N bond in IM7 is manifested to be impossible due to the high stability of IM7.

Another rearrangement of IM5 is the migration of Cl atom from C^2 to N *via* transition state TS10. During the migration process, the C^1–N double bond in IM5 is lengthened to a single bond while the single C^2–N bond is shortened to a double bond resulting in intermediate IM9 which easily decomposes to the end products ClNCO + CCl_2.

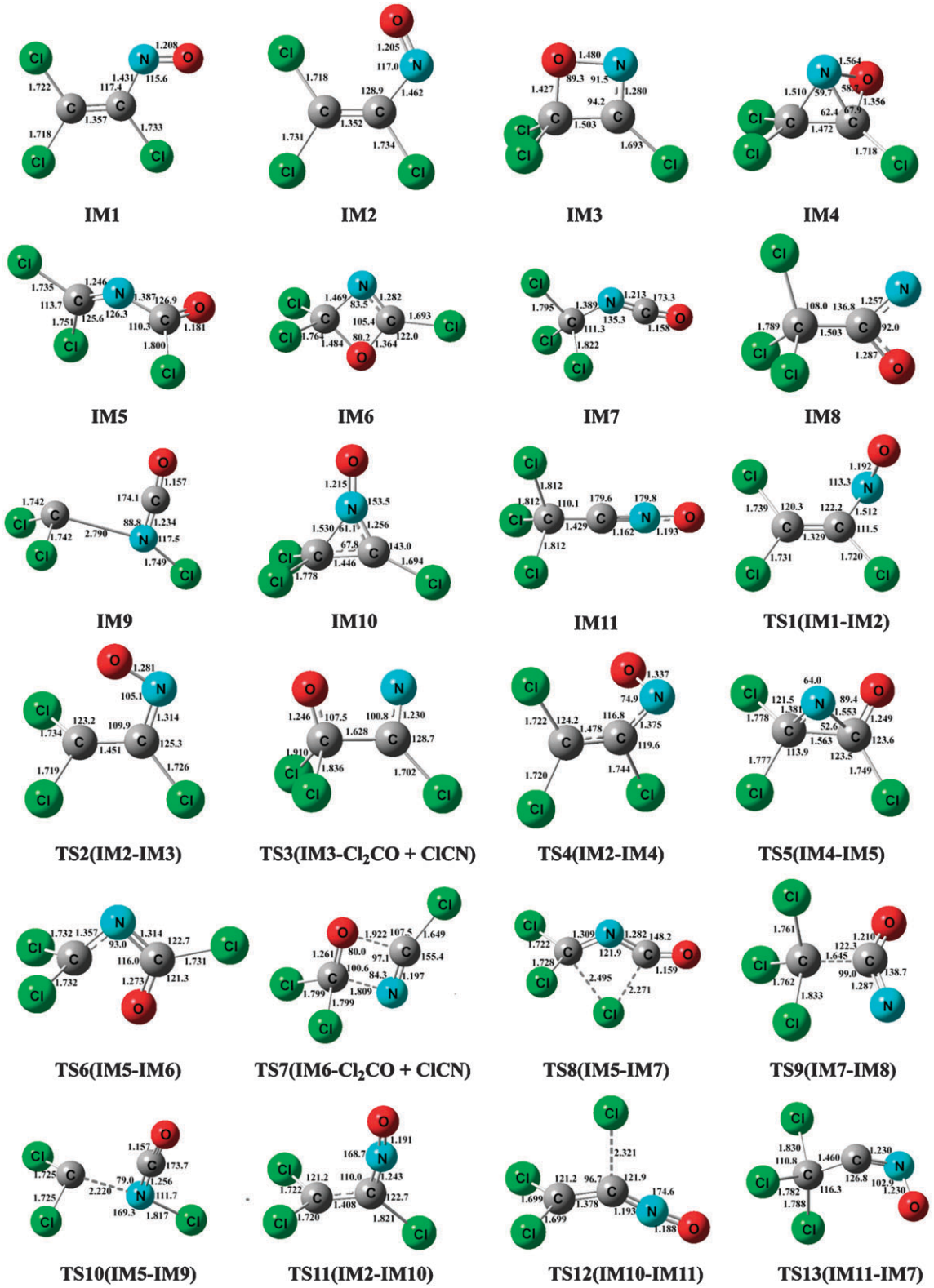

Fig. 1 Structures of the intermediates (IM) and the transition states (TS) involved in the C_2Cl_3 + NO reaction. Selected geometrical parameters obtained at the B3LYP/6-311G(d) level are shown. Bond distances are in angstroms and bond angles are in degrees.

Pathways *via* three-membered ring IM10

Another reaction route starting from the initial adduct *cis*-IM2 involves the formation of three-membered ring (CCN) isomer IM10 through the transition state TS11. The valence of N atom of this cyclic intermediate IM10 has been extended from three to five and the energy of IM10 is higher than the

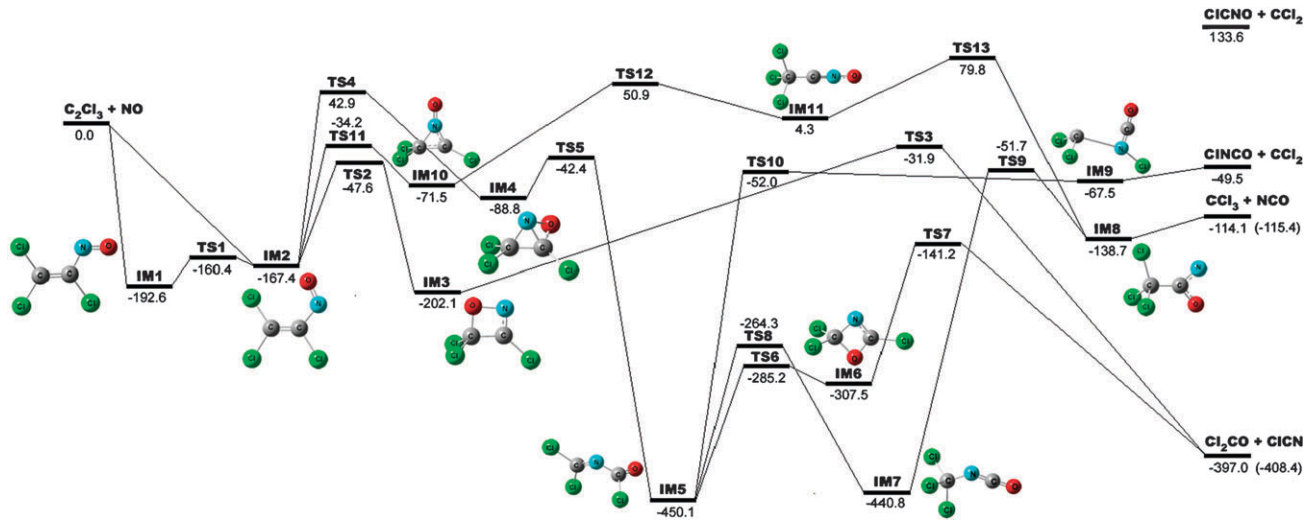

Fig. 2 Profiles of the potential energy surface for the C_2Cl_3 + NO reaction. The indicated energies (in kJ mol^{-1}) are obtained at the CCSD(T)/6-311 + G(d)//B3LYP/6-311G(d) level of calculation. The data in brackets are the experimental heats of reaction obtained using the data in NIST webbook (http://webbook.nist.gov/chemistry/). All the energies given are relative to the reactants and structures of crucial reaction intermediates are also depicted.

other two cyclic isomers, *i.e.*, the four-membered ring IM3 and the bicyclic IM4, for the three-membered ring has larger strain than the other two. IM10 may decyclize to open-chain isomer CCl_3CNO (IM11) through the transition state TS12. The energy of CCl_3CNO is a little higher than the reactants and is quite unstable compared to another open-chain isomer CCl_3NCO (IM7). Through TS13, IM11 can transform to $CCl_3C(N)O$ (IM8) which dissociates to the end products of CCl_3 + NCO. For this reaction pathway *via* the three-membered ring intermediate, the energies of the intermediates and transition states involved are much higher than that from the other two pathways *via* the four-membered ring or bicyclic ring intermediates. Therefore, the three-membered ring intermediate pathway appears to be energetically much less competitive.

Overall, the above calculations predict three reaction pathways, *i.e.*, pathways *via* four-membered ring, bicyclic ring, or three-membered ring intermediates. Four accessible product channels may result and the energies released from these three exothermic channels are 397.0 kJ mol^{-1} for Cl_2CO + ClCN, 440.8 kJ mol^{-1} for CCl_3NCO, 49.5 kJ mol^{-1} for ClNCO + CCl_2, and 114.1 kJ mol^{-1} for CCl_3 + NCO, respectively. In addition, an endothermic reaction channel leading to ClCNO + CCl_2 with the energy 133.6 kJ mol^{-1} higher than the reactants is also found, which is obviously not thermodynamically accessible and the detailed reaction route is not shown in Fig. 2 for clarity. Among the three reaction pathways, the four-membered ring intermediate pathway leading to the products Cl_2CO + ClCN should be the most kinetically and energetically favourable because it involves the least molecular rearrangements and the energies of all the transition states are all well below the reactants, which is essentially barrierless. In view of the other two pathways *via* the bicyclic ring or three-membered ring intermediates, they are rate-limited by large energy barriers (*i.e.*, TS4 and TS 13 lying 42.9 kJ mol^{-1} and 79.8 kJ mol^{-1} higher than the reactants, respectively) and thus expected to be much less competitive, resulting in minor yields of the corresponding products ClNCO + CCl_2, CCl_3NCO, and CCl_3 + NCO. These results predict that at room temperature Cl_2CO + ClCN should be the dominant channel. However if the reaction proceeds at high temperature and the reactants are supplied with sufficient available energies to surmount the large energy barriers, the product branching ratios of the other reaction channels, CCl_3 + NCO, CCl_3NCO, and ClNCO + CCl_2, should increase, *i.e.*, these channels will play more significant roles while Cl_2CO + ClCN will become less important. The predicted product channels and variation of branching ratios with energy will be detected by the following experiments.

Experimental observation of the reaction products

Experiments of time-resolved Fourier transform infrared emission (TR-FTIR) spectroscopy combining with laser photolysis are performed to observe the reaction products and the reaction pathways in competition with each other. C_2Cl_3 radicals are generated by excimer laser photolysis of the precursor C_2Cl_4 and they are the only reactive radicals produced from the photolysis.[6] Two laser wavelengths, 248 and 193 nm, are used to generate the C_2Cl_3 radicals with different internal energy. The laser fluence dependence of product yields have been measured in the intensity range from 4.2 to 9.6 × 10^6 W cm^{-2}. The measured slope of the fluence dependence is 1.2 ± 0.2 and 1.1 ± 0.2 at 248 nm and 193 nm, respectively, indicating that only one photon dissociation process occurs. Besides the radical C_2Cl_3, there exist some possibly interfering photofragments: Cl atoms, Cl_2 and C_2Cl_2 molecules. The reaction of Cl atoms with NO occurs *via* three-body association with a termolecular rate constant of 9.0 × 10^{-32} cm^6 $molecule^2$ s^{-1}.[24] Under the present total pressure of 70 Pa, it is estimated that the three-body association

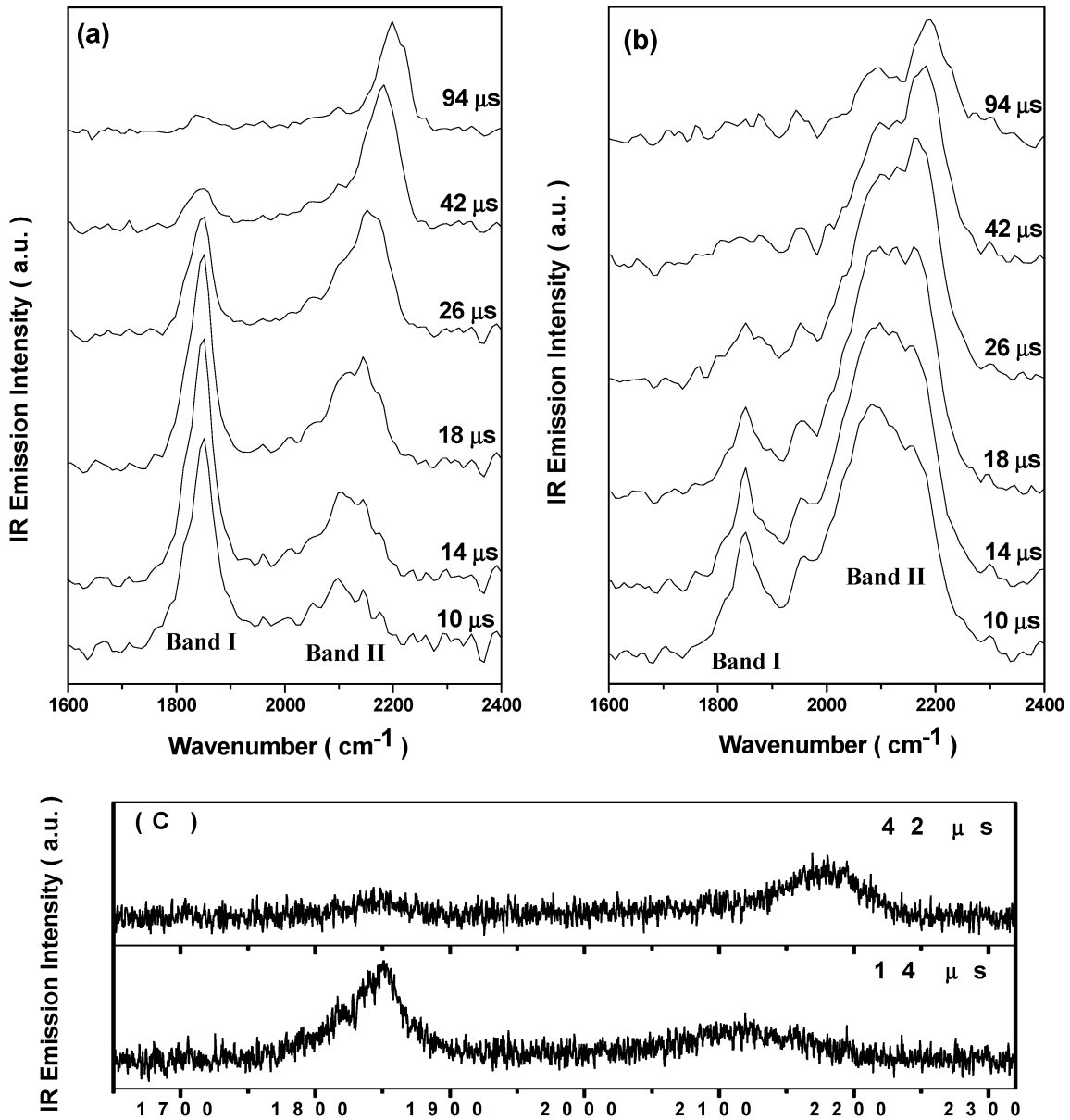

Fig. 3 Product TR-FTIR emission spectra from the reaction of C_2Cl_3 + NO taken at typical delay times from 10 μs to 94 μs after initiation of the reaction by an excimer laser at 248 nm (a) and 193 nm (b) collected using the InSb detector at a spectral resolution of 16 cm^{-1}, (c) is the higher resolution (0.5 cm^{-1}) spectra obtained at 248 nm.

reaction occurs slowly on a time scale of hundreds of milliseconds. The other photofragments, the chlorinated acetylene C_2Cl_2 and Cl_2 are stable molecules. Although Cl_2 may react with NO *via* bimolecular process, the reaction occurs slowly even at high temperature, *e.g.*, $k = 1.74 \times 10^{-18}$ cm^3 $molecule^{-1}$ s^{-1} at $T = 673$ K.[25] The reaction rate constant of C_2Cl_2 with NO was not measured before but it should be as slow as for the analogous C_2H_2 + NO reaction, which occurs with a rate constant of 2.07×10^{-24} cm^3 $molecule^{-1}$ s^{-1} at $T = 673$ K.[26] Consequently, all the co-existing photofragments Cl atoms, Cl_2 molecules, and chlorinated acetylenes C_2Cl_2 are not likely to compete with the highly reactive C_2Cl_3 radicals in their reaction with NO molecules (the reaction rate constant of C_2Cl_3 radical with NO was not measured before but it should be comparable to the analogous C_2H_3 + NO reaction, with the room temperature reaction rate constant reported[17] to be $(1.6 \pm 0.4) \times 10^{-11}$ cm^3 $molecule^{-1}$ s^{-1}). The photodissociation of C_2Cl_4 molecules provides a good source of C_2Cl_3 radicals for the study of its consecutive reaction with NO.

$$C_2Cl_4 \xrightarrow{h\nu} C_2Cl_3 + Cl$$
$$\rightarrow C_2Cl_2 + Cl_2$$

Based on previous photodissociation studies, the energy of the reactant, *i.e.*, the photolytically produced C_2Cl_3 radicals, can be first estimated as follows. UV absorption spectra measured by Berry[27] show that chloroethylenes C_2H_3Cl, $C_2H_2Cl_3$, C_2HCl_3 and C_2Cl_4 all have two absorption bands

in a region between 260 and 140 nm. A broad absorption band at ~200 nm is assigned to the $\pi^* \leftarrow \pi$ transition. Both 193 and 248 nm excitation falls into this absorption band, corresponding to the $\pi^* \leftarrow \pi$ transition. Except for C_2Cl_4, the photodissociation of a series of chloroethylenes including C_2H_3Cl, $C_2H_2Cl_2$ and C_2HCl_3 has been well studied with photofragment ion imaging or photofragment translation spectroscopy.[28–33] These studies have demonstrated that following the $\pi^* \leftarrow \pi$ transition at 193 nm, the photodissociation mechanisms for various chloroethylenes are basically the same, and the dominant pathway is the C–Cl bond rupture through predissociation *via* the crossing of the $\pi\pi^*$ state with the repulsive $\pi\sigma^*$ state, to give rise to fast Cl atoms. The measured average translational energy fraction ranges from 43.4, 42.2 and 36.6% for C_2H_3Cl, $C_2H_2Cl_2$ and C_2HCl_3 photodissociation, respectively. The photodissociation of C_2Cl_4 should follow the same mechanism as other chloroethylenes and thus the translational energy release can be evaluated to be most similar to that of C_2HCl_3, though perhaps a little smaller according to the trend shown with the Cl-substitution. Supposing 36% of energy released into the translation, the average internal energy of the C_2Cl_3 radicals can be estimated to be 62.3 kJ mol^{-1} at 248 nm and 150.6 kJ mol^{-1} at 193 nm, respectively. Evidently, the internal energy content of C_2Cl_3 radicals is greatly increased from 248 to 193 nm. At both wavelengths, hot C_2Cl_3 radicals with significant vibrational excitation are involved in the consecutive reaction with NO molecules. However, no IR emission signal due to vibrationally excited C_2Cl_3 radicals was detected in the TR-FTIR spectra in the reference experiments of the 248 or 193 nm photolysis of pure C_2Cl_4. The reason is that all the vibrational modes of C_2Cl_3 are below 1800 cm^{-1}, which is beyond the spectral detection range of InSb. This provides a background free detection of the reaction of C_2Cl_3 with NO_2.

Once the gaseous mixture of 10 Pa C_2Cl_4 with 60 Pa NO was irradiated by the excimer laser, strong IR emissions were observed as shown in Fig. 3. These IR emission bands are originated from the vibrationally excited products of the C_2Cl_3 + NO reaction. The spectra were collected with resolutions set at 16 and 0.5 cm^{-1}, respectively. There are basically two broad IR emission bands spanning 1740 to 1920 cm^{-1} (band I) and 2000 to 2300 cm^{-1} (band II), respectively, in the 16 cm^{-1} resolution spectra. As shown in Fig. 3(c), these two bands are rotationally irresolvable at the spectral resolution of 0.5 cm^{-1}, suggesting that they are not originated from diatomic products of NO and CO although their IR bands also fall within these spectral ranges, because rotationally resolved structure should be well resolved for NO and CO at 0.5 cm^{-1}.[11] Instead, these unresolved bands should be ascribed to polyatomic molecules. The assignment of these structureless bands is made possible with the aid of our theoretical calculations which have predicted the feasible reaction products.

IR emission spectra record the infrared fluorescence emitted from vibrationally excited species due to a set of vibrational transitions $\nu \rightarrow \nu - 1$ and thus the band is generally much broader than normal static IR absorption spectra and the peak center exhibits somewhat red shift relative to the fundamental frequency position ($1 \rightarrow 0$). According to its spectral position, the intense emission band from 1740 to 1920 cm^{-1} (band I) are most likely ascribed to the C–O stretching mode of Cl_2CO (fundamental frequency at 1827 cm^{-1}), which are predicted to be the major products theoretically. This IR emission band due to Cl_2CO has also been observed in the reaction of C_2Cl_3 with O_2[9] and NO_2[11] in our previous studies. The assignment of this band to another possible species with fundamental frequency at 1884 cm^{-1}, ClCO,[34] can be ruled out. First, none of the theoretically calculated feasible reaction pathways can lead to the product ClCO. Secondly, the possible channels corresponding to ClCO, *i.e.*, ClCO + CCl_2 + N (ΔH = 322.1 kJ mol^{-1}) or ClCO + CN + Cl_2 (ΔH = 46.0 kJ mol^{-1}), are all endothermic and obviously not thermodynamically accessible.

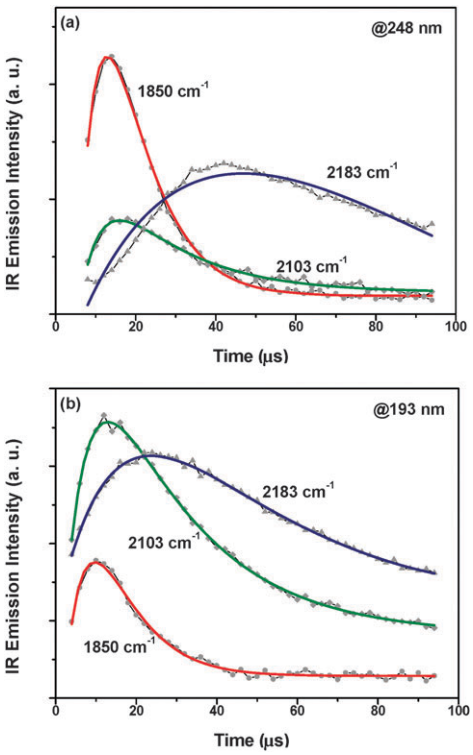

Fig. 4 Temporal evolution of several selected infrared emission peaks (1850, 2103 and 2183 cm^{-1}). The experimental data (dotted lines) are fitted with the biexponential rate function and plotted as solid lines. The IR emission intensities of the peaks are obtained from the spectra collected using the InSb detector at a spectral resolution of 16 cm^{-1}: (a) at 248 nm and (b) at 193 nm.

The other emission band spanning from 2000 to 2300 cm^{-1} (band II) at 248 nm undergoes apparent blue-shift with increasing time while its intensity grows, which is abnormal considering the fact that vibrational relaxation should result in the decreasing of the IR emission intensity as the band blue-shifts and cascades toward the band origin. This indicates that the broad 2000–2300 cm^{-1} band actually arises from two species with distinct time evolution. Fig. 4 depicts the temporal evolution of three selected infrared emission peaks (1850, 2103 and 2183 cm^{-1}). From Fig. 4, it is clearly seen that the 2183 cm^{-1} peak exhibits different kinetics from the peak at 2103 cm^{-1}, suggesting further that the 2000–2300 cm^{-1} band is due to two infrared emitting molecules which are peaked at 2103 and 2183 cm^{-1}, respectively. Moreover, as shown in

Fig. 3(b), when the photolysis laser is changed from 248 nm to 193 nm, the splitting of this band to two components with peaks at 2103 and 2183 cm^{-1} is more obviously discerned. Relative to the Cl_2CO band peaked at 1850 cm^{-1}, the intensity of the 2000–2300 cm^{-1} band becomes much stronger at 193 nm than that at 248 nm. It shows that the reaction products detected at 193 and 248 nm are basically identical while the relative product yields are varied remarkably.

To assist in assigning this illegible band II comprising two species peaked at 2103 and 2183 cm^{-1}, Table 1 lists the vibrational frequencies and Einstein A coefficients of the products and intermediates (IM) involved in the C_2Cl_3 + NO reaction calculated at the B3LYP/6-311G(d) level. By multiplying a scaling factor of 0.96, the calibrated frequencies using the B3LYP density functional method with the basis set 6-311G(d,p) are expected to agree well with the experimental fundamentals and provide a basis for the spectral assignment. As shown in Table 1, the calculated vibrational frequencies are well consistent with the experimental values for most species. Judging from the vibrational frequencies, the reaction products of ClCN, ClNCO, ClCNO are possibly related to the 2103 cm^{-1} peak. ClCNO can be first excluded since this product arises from a thermodynamically inaccessible channel as shown in Fig. 2. Second, this peak is not ascribed to ClCN since ClCN is the co-product of Cl_2CO which should also have a decreased yield at 193 nm. However, the intensity of this peak is greatly enhanced at 193 nm compared to that at 248 nm. In addition, ClCN corresponds to very small Einstein A coefficient (25.8 s^{-1}) as shown in Table 1 and thus is expected to give rise to very weak IR emission signals. In contrast, the product ClNCO corresponds to much larger Einstein A coefficient (506.4 s^{-1}) and arises from an energetically feasible channel. The 2103 cm^{-1} peak can be safely assigned to ClNCO. If there is some ClCN buried in the band of the strong emitter ClNCO, the contribution of ClCN to the fairly strong IR emission band of 2103 cm^{-1} is negligible.

It is noticeable in Fig. 4 that the 2183 cm^{-1} peak reaches its maximum intensity much more slowly than those of the other two peaks at 1850 and 2103 cm^{-1}, both at 248 and 193 nm. This implies that the 2183 cm^{-1} peak should correspond to a reaction intermediate which can be collision-stabilized at later time and thus grows to maximum intensity more slowly than the bimolecular reaction products, the Cl_2CO with its band peaked at 1850 cm^{-1} and another product ClNCO at 2103 cm^{-1}. Among all the [C_2, Cl_3, N, O] intermediates involved in the reaction, the open-chain isomers CCl_3NCO and CCl_3CNO have the vibrational frequencies falling close to the 2183 cm^{-1} peak as shown in Table 1. However, our theoretical calculations have shown that the formation of the highly unstable species CCl_3CNO is an endothermic process (ΔH = 4.3 kJ mol^{-1}) and thus CCl_3CNO is ruled out. Comparatively, the intermediate CCl_3NCO falls around the global minimum of the potential energy surface while facing a large exit barrier of dissociation. Therefore, the highly stable intermediate CCl_3NCO is the most likely species which can be collision-stabilized and thus captured in the IR spectra corresponding to the 2183 cm^{-1} peak. Furthermore, CCl_3NCO has the largest Einstein A coefficient (844.8 s^{-1}) among all the possible products and intermediates, which enhances greatly the probability of observing this species in the IR emission spectra.

Overall, the assignment of the broad band II comprising two species of ClNCO and CCl_3NCO peaked, respectively, at 2103 and 2183 cm^{-1} is quite reasonable if considering the fact that the structure with the XNCO sequence generally has the largest stability among the [X, C, N, O] isomers according to our calculations for X = Cl, CCl_3 and earlier findings for X = H, CH_3.[16,41] The calculated fundamental frequency (1 → 0 transition) of 2202 and 2280 cm^{-1} for ClNCO and CCl_3NCO, respectively, well fit both the observed peak positions of 2103 and 2183 cm^{-1}.

In addition, as shown in Fig. 3(b), when the photolysis laser is changed from 248 to 193 nm, a small peak at 1951 cm^{-1} can be identified in between the intense band I and band II. While at 248 nm, there is no obvious signal at this position. Based on the calculated frequencies listed in Table 1, this weak band is most likely ascribed to NCO which is also a feasible reaction product according to our theoretical calculations. Because of its small Einstein A coefficient (29.7 s^{-1}), NCO exhibits only a weak peak which can be barely discerned in between the neighbouring two strong bands. Since its IR band does not overlap with any other product species, NCO can still be observed although with small Einstein A coefficient.

Table 1 Experimental and calculated fundamental vibrational frequencies (cm^{-1}), and Einstein spontaneous emission coefficients $A(1 \rightarrow 0)$ (s^{-1}) of the products and intermediates (IM) involved in the C_2Cl_3 + NO reaction calculated at the B3LYP/6-311G(d) level

Species	ν(expt)[34–40]	ν(calc)	$A(1 \rightarrow 0)$	Vib. mode
Cl_2CO	1827	1822.0	158.3	C–O
ClCO	1885	1895.4	71.3	C–O
ClCN	2216	2223.7	25.8	C–N
ClNCO	2212	2201.9	506.4	N–C–O
ClCNO	2281	2325.9	211.7	C–N
NCO	1921	1919.2	29.7	N–C–O
IM5	—	1805.1	174.7	C–O
IM7	—	2280.2	844.8	C–N
IM10	—	1801.2	98.0	C–N
IM11	—	2358.6	673.0	C–N–O

Possible secondary reactions and their effects on the observed emission spectra

Although it is a versatile and powerful means of observing the IR-active products in a reaction mixture, the IR emission detection has the disadvantage of low sensitivity relative to other detection methods. Thus, the species partial pressures are necessarily relatively high to ensure adequate signal-to-noise ratios for detection purposes.[18] To minimize the secondary reactions of C_2Cl_3 radicals, we have maintained the NO concentration much larger than that of the C_2Cl_3 radicals (C_2Cl_3 concentration estimated to be ~10–100 times less than the NO concentration according to the absorption cross section of the precursor C_2Cl_4 at 248 and 193 nm).[24]

Fig. 4 plots the temporal evolution curves of the three major products Cl_2CO, ClNCO and CCl_3NCO. The rise reflects the product formation and the decay is due to vibrational relaxation and removal from the observation zone. The diffusion causing the removal from the observation zone occurs on the time

scale of hundreds of μs and thus can be neglected.[10] Therefore, the rise and fall of the IR emission temporal curves are fitted with a sum of two exponentials $y_0 + C(\exp(-k_1 t) - \exp(-k_2 t))$, providing information of the kinetics of the product formation and vibrational relaxation. Under this simplified model, satisfactory fitting results are obtained as shown in Fig. 4.

The biexponential fitting yields a pseudo-first-order formation rate constant of 1.1 (±0.2) × 10^{-11} cm^3 $molecule^{-1}$ s^{-1} for Cl_2CO, 1.6(±0.3) × 10^{-11} cm^3 $molecule^{-1}$ s^{-1} for ClNCO, and 1.8(±0.6) × 10^{-12} cm^3 $molecule^{-1}$ s^{-1} for CCl_3NCO, respectively, at 248 nm photolysis, and these values are increased to 2.0 (±0.1) × 10^{-11} cm^3 $molecule^{-1}$ s^{-1}, 2.9(±0.2) × 10^{-11} cm^3 $molecule^{-1}$ s^{-1}, and 3.5(±0.5) × 10^{-12} cm^3 $molecule^{-1}$ s^{-1}, respectively, at 193 nm because of more excess energy. There were no measurements of the reaction rate constant of C_2Cl_3 + NO previously in the literature. Presumably, the reaction rate of C_2Cl_3 + NO should be close to its counterpart reaction, C_2H_3 + NO, which has a room-temperature rate constant of $1.6 \pm 0.4 \times 10^{-11}$ cm^3 $molecule^{-1}$ s^{-1}.[17] Obviously, the derived formation rate constants of Cl_2CO and ClNCO agree well with the presumed reaction rate constant for the C_2Cl_3 + NO reaction, indicating that Cl_2CO and ClNCO are the primary products of the C_2Cl_3 + NO reaction. For the product CCl_3NCO, its formation rate constant of 1.8(±0.6) × 10^{-12} cm^3 $molecule^{-1}$ s^{-1} is one order of magnitude smaller than the overall reaction rate constant of C_2Cl_3 + NO. One possibility is that CCl_3NCO is from the three-body association reaction of C_2Cl_3 + NO which requires the product to be sufficiently stabilized at later reaction time and thus the formation rate is slower than the bimolecular reaction products of Cl_2CO and ClNCO, as we have suggested in the spectral assignment. The other possibility is that CCl_3NCO may arise from secondary reactions, *i.e.*, the consecutive reaction of the primary products causing the formation delay of CCl_3NCO. However, the possible secondary reactions which should occur mainly between the primary radical products (CCl_3, CCl_2 and NCO) and the abundant NO or C_2Cl_4 molecules can be eliminated as sources of this product as follows (secondary radical–radical reactions are negligible due to the low concentration of radicals).

For the association reactions of CCl_3 + NO, CCl_2 + NO, and NCO + C_2Cl_4 which are only of importance at pressures of several hundreds to thousands of Pa, they are expected to occur with negligible probability considering the low pressure of the present experiments (70 Pa).[42–44] The highly reactive NCO + NO reaction ($k = 3.36 \times 10^{-11}$ cm^3 $molecule^{-1}$ s^{-1} at room temperature)[45] does not coincide with the formation rate constant of CCl_3NCO ($k = 1.8 \times 10^{-12}$ cm^3 $molecule^{-1}$ s^{-1}) observed in the experiment. Furthermore, NCO was actually observed as a very minor product and thus its secondary reactions are not expected to give rise to detectable IR emissions. The possible CCl_3 + C_2Cl_4 and CCl_2 + C_2Cl_4 reactions simply do not yield products with vibrational frequencies within the current spectral detection range. From the above analysis, it can be elucidated that the major product species observed in the IR emission spectra arise from the primary reaction of C_2Cl_3 + NO, but not secondary reactions.

Branching ratios varied with reactant energy among competitive reaction pathways

Basically, there are four reaction products, Cl_2CO, ClNCO, NCO and CCl_3NCO observed in the TR-FTIR spectra, which can be associated to three bimolecular reaction channels: Cl_2CO of the channel Cl_2CO + ClCN, ClNCO of the channel CCl_2 + ClNCO, and NCO of the channel CCl_3 + NCO, as well as one combination reaction channel forming the collision-stabilized adduct CCl_3NCO. To estimate the branching ratios of these channels, the product IR emission intensities (denoted by maximum peak heights) are corrected by two factors. One is the instrumental response function which reflects mainly the spectral response of the detector varied with the IR frequency within the broad spectral range that the four products cover from 1800 to 2300 cm^{-1}. The instrumental response function was measured using a black-body source (Gemini R Model 976, Isothermal Technology LTD) maintained at 773 K.[9] The other factor is the product Einstein *A* coefficient which can be obtained from the *ab initio* calculations. Table 1 lists the Einstein *A* coefficients for the fundamental frequencies (1 → 0 transitions) calculated at the B3LYP/6-311G(d) level. For the broad IR emission bands comprising several products from 1800 to 2300 cm^{-1}, the contribution of each species are weighed by their Einstein *A* coefficients. By this means, the relative product yields and branching ratios of each channel can be estimated and the results are listed in Table 2.

As shown in Table 2, the Cl_2CO channel obviously dominates the total reaction, accounting for a branching ratio of 90.2% at 248 nm and 56.5% at 193 nm. This agrees very well with the theoretical calculation results showing that Cl_2CO arises from the essentially barrierless four-membered ring intermediate pathway which is the most kinetically and energetically favourable among all the possible pathways. In contrast, the other two products ClNCO and CCl_3NCO only accounts for minor yields at 248 nm. As pointed out in our calculation results, these two products are both generated from the bicyclic ring intermediate pathway which is rate-limited by a barrier of surmounting TS4 which lies 42.9 kJ mol^{-1} higher than the reactants. With an internal energy of 62.3 kJ mol^{-1} when produced by 248 nm photolysis, the reactant C_2Cl_3 radicals possess just enough energy to surmount this barrier and thus the products ClNCO and CCl_3NCO are observed in the IR emission spectra but with very low yields (9.7% in total). While the reactant C_2Cl_3 radicals are partitioned with significantly increased internal energy of 150.6 kJ mol^{-1} at 193 nm, this rate-limited barrier of 42.9 kJ mol^{-1} is well below the energy of the reactants and the bicyclic ring intermediate pathway is thus greatly enhanced. Correspondingly, the branching ratios of the two products ClNCO and CCl_3NCO are remarkably increased to a total of 43.5% at 193 nm, almost accounting for half of the product yields.

Table 2 Derived branching ratios (%) of three main product channels at 248 and 193 nm. The branching ratios have been normalized assuming these channels account for the total reaction

Branching ratio	Cl_2CO	ClNCO	CCl_3NCO
At 248 nm	90.3	5.8	3.9
At 193 nm	56.5	27.8	15.7

Primarily, the experimental evaluation of the branching ratios shows that the Cl_2CO channel *via* the four-membered ring intermediate pathway is overwhelmingly dominant at low energy (temperature) but becomes less important at high energy when the ClNCO and CCl_3NCO channels *via* the bicyclic ring intermediate pathway are enhanced and compete effectively. The observed variation of the branching ratios with energy among competitive reaction pathways consists nicely with the calculated potential energy profiles, providing further experimental evidence that the reaction proceeds through the key intermediates of four-membered and bicyclic ring adducts.

Among the four observed products, NCO corresponds to a weak emission band superimposed on top of the intense bands of Cl_2CO (band I) and ClNCO/CCl_3NCO (band II). While the other bands are quenched due to vibrational relaxation at later time, the NCO band becomes quite noisy. Thus, it is hard to estimate its band intensity under this situation. For this reason, the relative yields and branching ratios are not given for NCO as for other intense products listed in Table 2. Nevertheless, this treatment does not affect the estimation of the branching ratios with other products. It can be expected that the product yields of NCO is negligible because the signal of NCO can barely be discerned at 193 nm while not detected at all at 248 nm.

Conclusions

In summary, the products and mechanisms of the C_2Cl_3 + NO reaction are investigated comprehensively by step-scan time-resolved Fourier transform infrared emission spectroscopy and CCSD(T)/6-311+G(d)//B3LYP/6-311G(d) level of electronic structure calculations. Vibrationally excited products of Cl_2CO, ClNCO, CCl_3NCO and NCO have been observed in the IR emission spectra. Cyclic intermediates are found to play important roles leading to the rich variety of the chemical transformation of the title reaction. There are mainly two competitive reaction pathways revealed: (1) the four-membered ring intermediate pathway leading to the products Cl_2CO + ClCN which is essentially barrierless and should be the most kinetically and energetically favourable pathway at room temperature; (2) the bicyclic ring intermediate pathway leading to the product channels of ClNCO + CCl_2, CCl_3NCO, and CCl_3 + NCO which is rate-limited by a barrier of 42.9 kJ mol^{-1} higher than the reactants, and should be less competitive.

By photolyzing the precursor at 248 and 193 nm, respectively, C_2Cl_3 radicals with different internal energy are produced to study the product branching ratios as a function of energy among competitive reaction pathways. The branching ratios derived from the IR emission spectra shows that the Cl_2CO channel *via* the four-membered ring intermediate pathway is overwhelmingly dominant at low energy (temperature) but becomes less important at high energy when the ClNCO and CCl_3NCO channels *via* the bicyclic ring intermediate pathway are greatly enhanced and compete effectively. The nice agreement between the experimental observation of the product branching ratios variation with reactant energy and the calculated potential energy profiles indicates that the C_2Cl_3 + NO reaction proceeds primarily through these key cyclic intermediates, *i.e.*, the four-membered and bicyclic ring intermediates.

Compared to its counterpart C_2H_3 + NO reaction which has only one observed significant product channel, *i.e.*, HCN + H_2CO *via* the dissociation of the four-membered ring intermediate, the C_2Cl_3 + NO reaction exhibits a variety of competitive channels involving not only the four-membered ring intermediate, but also the bicyclic ring intermediate pathways. The reason leading to the different chemistry of these two seemingly similar reactions is currently under investigation.

Acknowledgements

This work is financially supported by the National Natural Science Foundation of China (Grant No#20733005, No#20973179 and No#20903104), and the National Basic Research Program of China (2007CB815200, 2007AA02Z116).

References

1 S. M. Senkan, J. M. Robinson and A. K. Gupta, *Combust. Flame*, 1983, **49**, 305–314.
2 H. Valeiras, A. K. Gupta and S. M. Senkan, *Combust. Sci. Technol.*, 1984, **36**, 123–133.
3 P. H. Taylor, D. A. Tirey, W. A. Rubey and B. Dellinger, *Combust. Sci. Technol.*, 1994, **101**, 75–102.
4 P. H. Taylor, D. A. Tirey and B. Dellinger, *Combust. Flame*, 1996, **107**, 193–195.
5 L. Sorum, O. Skreiberg, P. Glarborg, A. Jensen and K. Dam-Johansen, *Combust. Flame*, 2001, **124**, 195–212.
6 J. J. Russell, J. A. Seetula, D. Gutman and S. M. Senkan, *J. Phys. Chem.*, 1989, **93**, 1934–1938.
7 S. A. Kostina, M. G. Bryukov, A. A. Shestov and V. D. Knyazev, *J. Phys. Chem. A*, 2003, **107**, 1776–1778.
8 H. Wang, J. C. Li, X. L. Song, Y. Z. Li, H. Hou, B. S. Wang, H. M. Su and F. N. Kong, *J. Phys. Chem. A*, 2006, **110**, 10336–10344.
9 T. C. Xiang, K. H. Liu, S. L. Zhao, H. M. Su, F. N. Kong and B. S. Wang, *J. Phys. Chem. A*, 2007, **111**, 9606–9612.
10 T. C. Xiang, K. H. Liu and H. M. Su, *Chin. J. Chem. Phys.*, 2007, **20**, 407–411.
11 K. H. Liu, T. C. Xiang, W. Q. Wu, S. L. Zhao and H. M. Su, *J. Phys. Chem. A*, 2008, **112**, 10807–10815.
12 A. G. Sherwood and H. E. Gunning, *J. Phys. Chem.*, 1965, **69**, 1732–1736.
13 A. G. Sherwood and H. E. Gunning, *J. Am. Chem. Soc.*, 1963, **85**, 3506–3508.
14 S. W. Benson, *Int. J. Chem. Kinet.*, 1994, **26**, 997–1011.
15 S. Arulmozhiraja and P. Kolandaivel, *THEOCHEM*, 1998, **429**, 165–173.
16 R. Sumathi, H. M. T. Nguyen, M. T. Nguyen and J. Peeters, *J. Phys. Chem. A*, 2000, **104**, 1905–1914.
17 F. Striebel, L. E. Jusinski, A. Fahr, J. B. Halpern, S. J. Klippenstein and C. A. Taatjes, *Phys. Chem. Chem. Phys.*, 2004, **6**, 2216–2223.
18 P. Zou, S. J. Klippenstein and D. L. Osborn, *J. Phys. Chem. A*, 2005, **109**, 4921–4929.
19 A. D. Becke, *J. Chem. Phys.*, 1993, **98**, 5648–5652.
20 C. T. Lee, W. T. Yang and R. G. Parr, *Phys. Rev. B: Condens. Matter*, 1988, **37**, 785–789.
21 C. Gonzalez and H. B. Schlegel, *J. Chem. Phys.*, 1989, **90**, 2154–2161.
22 M. J. Frisch, G. W. Trucks, H. B. Schlegel, G. E. Scuseria, M. A. Robb, J. R. Cheeseman, J. A. Montgomery, Jr., T. Vreven, K. N. Kudin, J. C. Burant, J. M. Millam, S. S. Iyengar, J. Tomasi, V. Barone, B. Mennucci, M. Cossi, G. Scalmani, N. Rega, G. A. Petersson, H. Nakatsuji, M. Hada, M. Ehara, K. Toyota, R. Fukuda, J. Hasegawa, M. Ishida, T. Nakajima, Y. Honda, O. Kitao, H. Nakai, M. Klene, X. Li,

J. E. Knox, H. P. Hratchian, J. B. Cross, V. Bakken, C. Adamo, J. Jaramillo, R. Gomperts, R. E. Stratmann, O. Yazyev, A. J. Austin, R. Cammi, C. Pomelli, J. Ochterski, P. Y. Ayala, K. Morokuma, G. A. Voth, P. Salvador, J. J. Dannenberg, V. G. Zakrzewski, S. Dapprich, A. D. Daniels, M. C. Strain, O. Farkas, D. K. Malick, A. D. Rabuck, K. Raghavachari, J. B. Foresman, J. V. Ortiz, Q. Cui, A. G. Baboul, S. Clifford, J. Cioslowski, B. B. Stefanov, G. Liu, A. Liashenko, P. Piskorz, I. Komaromi, R. L. Martin, D. J. Fox, T. Keith, M. A. Al-Laham, C. Y. Peng, A. Nanayakkara, M. Challacombe, P. M. W. Gill, B. G. Johnson, W. Chen, M. W. Wong, C. Gonzalez and J. A. Pople, *GAUSSIAN 03*, Gaussian, Inc., Wallingford, CT, 2004.

23 T. C. Xiang, K. H. Liu, C. Y. Shi, H. M. Su and F. N. Kong, *Chem. Phys. Lett*., 2007, **437**, 8–13.

24 R. Patrick and D. M. Golden, *Int. J. Chem. Kinet*., 1983, **15**, 1189–1227.

25 P. G. Ashmore and J. Chanmugam, *Trans. Faraday Soc*., 1953, **49**, 270–271.

26 H. M. T. Nguyen, R. Sumathi and M. T. Nguyen, *J. Phys. Chem. A*, 1999, **103**, 5015–5022.

27 M. J. Berry, *J. Chem. Phys*., 1974, **61**, 3114–3143.

28 M. Umemoto, K. Seki, H. Shinohara, U. Nagashima, N. Nishi, M. Kinoshita and R. Shimada, *J. Chem. Phys*., 1985, **83**, 1657–1666.

29 T. Suzuki, K. Tonokura, L. S. Bontuyan and N. Hashimoto, *J. Phys. Chem*., 1994, **98**, 13447–13451.

30 K. Tonokura, L. B. Daniels, T. Suzuki and K. Yamashita, *J. Phys. Chem. A*, 1997, **101**, 7754–7764.

31 K. Sato, S. Tsunashima, T. Takayanagi, G. Fujisawa and A. Yokoyama, *J. Chem. Phys*., 1997, **106**, 10123–10133.

32 D. A. Blank, W. Z. Sun, A. G. Suits, Y. T. Lee, S. W. North and G. E. Hall, *J. Chem. Phys*., 1998, **108**, 5414–5425.

33 Y. J. Lee, Y. R. Lee, C. C. Chou and S. M. Lin, *J. Chem. Phys*., 1998, **109**, 346–347.

34 S. H. Chen, L. K. Chu, Y. J. Chen, I. C. Chen and Y. P. Lee, *Chem. Phys. Lett*., 2001, **333**, 365–370.

35 M. E. Jacox, *J. Phys. Chem. Ref. Data*, 2003, **32**, 1–441.

36 J. S. Kwiatkowski and J. Leszczynski, *Mol. Phys*., 1994, **81**, 119–131.

37 W. J. Lafferty, D. R. Lide and R. A. Toth, *J. Chem. Phys*., 1965, **43**, 2063–&.

38 T. C. Devore, *J. Mol. Struct*., 1987, **162**, 287–304.

39 G. Maier and J. H. Teles, *Angew. Chem., Int. Ed. Engl*., 1987, **26**, 155–156.

40 C. E. Barnes, J. M. Brown, A. D. Fackerell and T. J. Sears, *J. Mol. Spectrosc*., 1982, **92**, 485–496.

41 A. M. Mebel, A. Luna, M. C. Lin and K. Morokuma, *J. Chem. Phys*., 1996, **105**, 6439–6454.

42 L. Ley, J. Masanet, F. Caralp and R. Lesclaux, *J. Phys. Chem*., 1995, **99**, 1953–1960.

43 A. A. Shestov, S. A. Kostina, E. V. Shafir, I. R. Slagle and V. D. Knyazev, *Chem. Phys. Lett*., 2003, **381**, 766–770.

44 K. H. Becker, R. Kurtenbach and P. Wiesen, *J. Phys. Chem*., 1995, **99**, 5986–5991.

45 D. L. Baulch, C. J. Cobos, R. A. Cox, P. Frank, G. Hayman, T. Just, J. A. Kerr, T. Murrells, M. J. Pilling, J. Troe, R. W. Walker and J. Warnatz, *J. Phys. Chem. Ref. Data*, 1994, **23**, 847–1033.

